Spatial structure and time evolution of the Weibel instability in collisionless inhomogeneous plasmas

F. Califano,[1] F. Pegoraro,[2] and S. V. Bulanov[3]
[1]*Scuola Normale Superiore, INFM (Forum), Pisa, Italy*
and Department of Astronomy, University of Florence, Florence, Italy
[2]*Department of Theoretical Physics and INFM, University of Turin, Turin, Italy*
and Department of Physics, University of Pisa, Italy
[3]*General Physics Institute, RAS, Moscow, Russia*
(Received 26 December 1996)

The magnetic field generated in an initially unmagnetized and anisotropic inhomogeneous plasma by the development of the Weibel instability is strongly nonuniform. For the case of a plasma where the anisotropy arises from two (relativistic) counterstreaming electron beams it is shown, both analytically and numerically, that this instability develops a spatial ''resonant''-type singularity. The largest magnetic field is generated around this singularity and has opposite polarities. In the case of one-dimensional (1D) perturbations, a current layer is formed very rapidly at the resonance position, almost independently of the characteristic scale of the initial perturbation. In 2D, numerical simulations show that a chain of current vortices is formed. [S1063-651X(97)10606-7]

PACS number(s): 52.35.Qz, 52.40.Nk, 52.60.+h, 52.65.Kj

I. INTRODUCTION

The Weibel instability [1–6] is an efficient mechanism of magnetic field generation in anisotropic plasmas. This instability also occurs in cold plasmas when the role of the anisotropy is played by two electron streams propagating in opposite directions. In this latter case, the physical mechanism which drives the instability can be described as follows. When the electric currents carried by the electron streams are displaced, one with respect to the other, by a transversal disturbance, the repulsion of the two oppositely directed currents reinforces the initial displacement. As a result, a larger and larger magnetic field is produced as time increases. The linear evolution of this electron instability and its nonlinear phase, before nonlinearities become so strong that they lead to self-intersection of the orbits of the electrons in each stream, can be described within the framework of a system of cold (relativistic) two-electron-fluid equations. If the time scales involved are sufficiently short, i.e., if the modes grow on a fast electron time scale, ions can be taken to be at rest. If the two electron components were treated as a single fluid and charge separation leading to electrostatic perturbations were excluded, these equations would reduce to the well known electron-magnetohydrodynamics (EMHD) equations [7].

The Weibel instability has been invoked in order to explain the generation of a magnetic field wake observed in particle in cell (PIC) simulations of the interaction of ultrashort and ultraintense laser pulses with an underdense plasma [8–10]. In this case the onset of the Weibel instability is related to the fast electron streams produced near the rear part of the laser pulse and behind it by the breaking of the Langmuir waves produced by the laser pulse. Due to the plasma quasineutrality, the average current of these energetic electrons must be canceled by an opposite current carried by electrons of the bulk plasma component. As mentioned above, these oppositely directed currents repel each other, making the distribution of the current density in the plasma inhomogeneous in the transverse direction and producing a quasistationary magnetic field.

In the astrophysical context, the ion Weibel instability driven by a cross-field current has been proposed as a mechanism for rapid current disruption phenomena observed in the magnetotail [11,12]. This work is motivated by observational evidence of substorm onset in regions where strong magnetic fields normal to the current sheet stabilize most of the instabilities generally invoked to explain strong energetic events. The ion Weibel instability is a very promising candidate for substorm initiation in such conditions [13].

The linear dispersion relation of the Weibel instability of two counter-streaming relativistic electron beams in a homogeneous plasma, for perturbations with wave vectors perpendicular to the stream direction, was presented in [14] together with an analysis of the nonlinear development of the instability in different wavelength regimes.

In the present paper we address the problem of the space and time development (mainly in the linear phase) of the Weibel instability in an inhomogeneous plasma where the electron streams are spatially nonuniform and the plasma density may vary in the direction perpendicular to the streams, as is the case, e.g., in the interaction of a laser pulse with a plasma mentioned above. In this inhomogeneous case, the electron equations develop a spatial singularity around which the magnetic field generated by the instability becomes more and more concentrated. In the simple case of one-dimensional perturbations in a uniform density plasma with two symmetric (equal densities and opposite velocities) nonuniform electron counterstreams, this ''Weibel singularity'' occurs at the position where twice the growth rate (normalized on the plasma frequency of one of the electron streams) matches the square of the local value of the electron velocity (normalized on the speed of light). As a result, a

mode strongly localized around the singularity develops from any initial perturbation at a rate which depends on the characteristic gradient of the electron velocities. The polarity of the magnetic field is opposite on the two sides of the singularity. A similar structure is also found to occur for two-dimensional perturbations which develop a localized chain of oppositely polarized magnetic domains. The characteristic spatial scale of the field produced by these localized instabilities is of the order of the electron skin depth. This can be understood by noting that this scale corresponds to the value of the wave number k for which the linear growth rate becomes largest and almost independent of k.

This paper is organized as follows. In Sec. II, we introduce the cold (relativistic) two-electron-fluid equations and present the main features of the Weibel instability in a homogeneous plasma by considering perturbations forming an arbitrary angle with the stream direction. In Sec. III we study the ''resonant'' behavior of the perturbation which arises in a plasma with nonuniform equilibrium electron velocities. As an illustration, we derive the spatial behavior around the resonant position of perturbations with given growth rate. For the sake of simplicity we consider perturbations that propagate perpendicularly to the two counterstreaming nonuniform electron streams and assume that these streams are symmetric and have nonrelativistic velocities. In addition, we take the plasma density to be homogeneous. In Sec. IV we consider an initial value problem and study the time evolution of an initially given perturbation. We follow the growth of the perturbation amplitude, its localization, and the formation of increasingly small spatial scales numerically, both for nonrelativistic and for relativistic electron streams. We analyze the case of one-dimensional as well as two-dimensional (2D) perturbations. In the latter case 2D vortices are formed in the current density accompanied by fine spatial structures in the density of the two electron beams. A brief discussion of the code used for the numerical simulations is given in the Appendix.

II. THE WEIBEL INSTABILITY

Assuming the ions to be at rest and to provide a uniform neutralizing background, we study the relativistic dynamics of the two electron counterstreaming populations in the fluid approximation by means of the following set of (dimensionless) equations:

$$\frac{\partial \mathbf{p}_a}{\partial t} = -\mathbf{v}_a \cdot \nabla \mathbf{p}_a - (\mathbf{E} + \mathbf{v}_a \times \mathbf{B}), \tag{1}$$

$$\frac{\partial n_a}{\partial t} = \nabla \cdot \mathbf{j}_a, \tag{2}$$

$$\frac{\partial \mathbf{B}}{\partial t} = -\nabla \times \mathbf{E}, \tag{3}$$

$$\frac{\partial \mathbf{E}}{\partial t} = \nabla \times \mathbf{B} - \sum_a \mathbf{j}_a, \tag{4}$$

$$\nabla \cdot \mathbf{E} = -\sum_a n_a, \tag{5}$$

with

$$\mathbf{v}_a = \frac{\mathbf{p}_a}{(1+p_a^2)^{1/2}}, \quad \mathbf{j}_a = -n_a \mathbf{v}_a, \quad a = 1,2 \tag{6}$$

where all the quantities are normalized on a characteristic density $\overline{n}$, on the speed of light c, and on the plasma frequency $\overline{\omega} = (4\pi \overline{n} \overline{e}^2/m)^{1/2}$. Notice that Eq. (5) is equivalent to a linear combination of Eqs. (2) and (4).

A. Homogeneous plasma

We can study the behavior of infinitesimal perturbations by linearizing the system of Eqs. (1)–(4). We consider a homogeneous plasma with velocities $v_{0,a}$ such that the net current density is zero,

$$\sum_a n_{0,a} v_{0,a} = 0. \tag{7}$$

As initially the plasma is nonmagnetized, the direction of the electron streams, parallel to the x axis of a Cartesian reference frame, is the only preferential direction. Without loss of generality, the evolution of any perturbation with wave vector $\mathbf{k}$ can therefore be studied in an (x,y) plane chosen so that the wave vector $\mathbf{k} = (k_x, k_y)$ lies in the plane itself. As is known, the Weibel instability generates a magnetic field B_z perpendicular to the plane (x,y). Then, assuming all perturbed quantities in the form

$$F(x,y,t) = f e^{i(k_x x + k_y y - \omega t)}, \tag{8}$$

and defining $\Omega_a = \omega - k_x v_{0,a}$ and $\Gamma_a = (1 - v_{0,a}^2)^{-1/2}$, the dispersion relation reads

$$(1-\Omega_2^{-2})[k_x^2(1+\Omega_4^{-2}) - \omega^2(1-\Omega_1^{-2}) - 2\omega k_x \Omega_3^{-2}] + k_y^2[(1-\Omega_1^{-2})(1+\Omega_4^{-2}) + \Omega_3^{-4}] = 0, \tag{9}$$

where

$$\Omega_1^{-2} = \sum_a \frac{n_{0,a}}{\Gamma_a \Omega_a^2}, \quad \Omega_2^{-2} = \sum_a \frac{n_{0,a}}{\Gamma_a^3 \Omega_a^2}, \tag{10}$$

$$\Omega_3^{-2} = \sum_a \frac{n_{0,a} v_{0,a}}{\Gamma_a \Omega_a^2}, \quad \Omega_4^{-2} = \sum_a \frac{n_{0,a} v_{0,a}^2}{\Gamma_a \Omega_a^2}.$$

Notice that, because of Eq. (7),

$$k_x^2(1+\Omega_4^{-2}) - \omega^2(1-\Omega_1^{-2}) - 2\omega k_x \Omega_3^{-2} = k_x^2 - \omega^2 + \sum_a \frac{n_{0,a}}{\Gamma_a}. \tag{11}$$

When the perturbation propagates parallel to the mean electron streams, i.e., $k_y = 0$, the electrostatic two-stream instability amplifies the perturbed electric field E_x with a growth rate obtained by solving the equation $1 - \Omega_2^{-2} = 0$. No magnetic field is produced in this case. In the opposite limit, $k_x = 0$, the dispersion relation reduces to (see [14], and references therein)

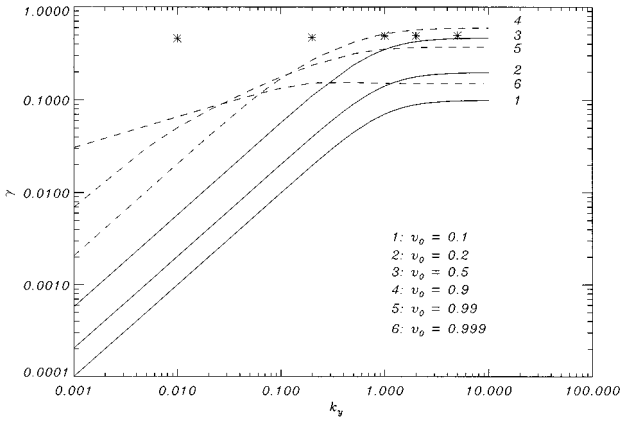

FIG. 1. Growth rate of the 1D Weibel instability versus the wave number k_y for a homogeneous plasma. Curves 1,2,3 (continuous lines) refer to three nonrelativistic symmetric cases ($v_{0,1}=-v_{0,2}=v_0$) with stream velocities $v_0=0.1,0.2,0.5$. Curves 4,5,6 refer to three relativistic symmetric cases with $v_0=0.9,0.99,0.999$. The stars are the growth rates of the Weibel instability in an inhomogeneous plasma (see Sec. IV) for five different wave numbers, $k_y=0.01,0.2,1,2,5$. In this figure and in the following ones dimensionless units are used.

$$\omega^2(1-\Omega_2^{-2})(1-\Omega_1^{-2}) - k_y^2[(1-\Omega_1^{-2})(1+\Omega_4^{-2})+\Omega_3^{-4}]=0. \quad (12)$$

Equation (12) contains two oscillatory solutions and one purely growing electromagnetic instability (1D Weibel instability) which amplifies any initial small magnetic perturbation.

In Fig. 1 (continuous lines) we plot the growth rate of the 1D Weibel instability versus the wave number k_y for three symmetric nonrelativistic cases ($v_{0,1}=-v_{0,2}=0.1$, 0.2, 0.5, continuous lines) and for three symmetric relativistic cases ($v_{0,1}=-v_{0,2}=0.9$, 0.99, 0.999, dashed lines). The stars represent the growth rates of the ''localized mode'' for a plasma with inhomogeneous electron streams (see Sec. IV). This figure shows that, in the nonrelativistic regime (continuous lines), the growth rate increases linearly with k_y for small values of k_y and saturates at $k_y\simeq 1$. In the relativistic limit (dashed lines) the slope of the curves is more and more reduced and, most important, saturation occurs at lower and lower values [i.e., $k_y\approx(\Gamma_a)^{-1/2}$], as consistent with the relativistic increase of the effective electron skin depth. For the same reason, the value of the maximum growth rate is also reduced in the strong relativistic case (curve 6).

The saturation of the Weibel instability with respect to the wave number k_y has important implications for the analysis of the time evolution of the instability in an inhomogeneous equilibrium that will be presented in the following sections. In the inhomogeneous case the spatial scale of the perturbations is formed dynamically and we may thus expect that the inhomogeneous growth rate will not increase significantly after the perturbation has reached a typical scale corresponding, in the nonrelativistic case, to $k\simeq 1$.

In the 2D case with intermediate propagation angles, i.e., for nonvanishing values of both k_x and k_y, the Weibel instability and the two-stream instability are coupled in a single branch. As is well known, the 1D two-stream instability has

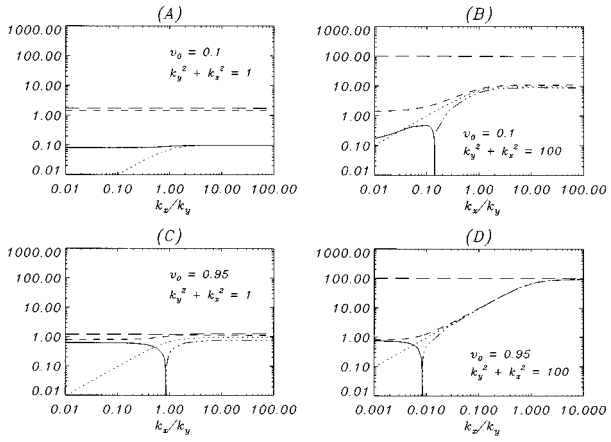

FIG. 2. Growth rate of the 2D instability (continuous lines) versus k_x/k_y in a homogeneous plasma and frequencies of the transverse e.m. and longitudinal Langmuir plasma waves (long and small dashed lines, respectively). The new mode of the 2D dispersion relation is shown by dotted lines and the stable continuation of the 2D instability by a dotted-dashed line [frames (B), (C), (D)]. The first two frames (A) and (B) belong to a nonrelativistic symmetric case, $v_0=0.1$ and the last two (C) and (D) to a relativistic symmetric case, $v_0=0.95$.

a cutoff ($k_x^{\max}$) beyond which the mode is stabilized. This cutoff depends on the stream velocity and, in 2D, on the modulus of the wave vector $(k_x^2+k_y^2)^{1/2}$, as shown in Fig. 2 by the continuous lines which represent the growth rate of the 2D instability versus the angle k_x/k_y. In this figure the first two frames (A) and (B) belong to a nonrelativistic symmetric case ($v_{0,1}=-v_{0,2}=0.1$), while the last two (C) and (D) belong to a relativistic symmetric case ($v_{0,1}=-v_{0,2}=0.95$); here Eq. (9) is solved on a circle of fixed radius $k_x^2+k_y^2=$ const. The cutoff of the coupled ''Weibel two-stream mode'' is seen in all frames apart from the case of low stream velocity and small values of the modulus of the wave vector [frame (A)]. Note that in the relativistic regime this cutoff occurs at lower values of k_x than in the nonrelativistic case. In Fig. 2 we also show the three stable branches of Eq. (9) corresponding to transverse [electromagnetic (e.m.)] and longitudinal (Langmuir) plasma waves.

III. NONHOMOGENEOUS PLASMA

In order to model the conditions where the electron streams are excited in the central region of the plasma, we assume that the inhomogeneity can be described as one dimensional along the y axis and write

$$\mathbf{p}_a=(p_{0,a}+p_{a,x},p_{a,y},0), \quad n_a=n_{0,a}+n_a, \quad (13)$$

$$\mathbf{E}=(E_x,E_y,0), \quad \mathbf{B}=(0,0,B_z), \quad (14)$$

where $p_{0,a}(y)$ and $n_{0,a}(y)$ are zero order (equilibrium) quantities such that, in agreement with Eq. (7), the total current $\Sigma_a j_{0,a}(y)=0$. For the sake of simplicity, in this section we assume equal and homogeneous mean electron density distributions

$$n_{0,1}=n_{0,2}=1, \quad v_{0,1}(y)=-v_{0,2}(y). \quad (15)$$

In this symmetric limit the y component of the electric field vanishes.

A. Local analysis

The occurrence of a singularity in the spatial structure of the Weibel instability in the case of inhomogeneous stream velocities is best seen by taking at first one-dimensional perturbations with given growth rate $\gamma \equiv -i\omega$ of the form

$$F(y,t) = f(y)e^{\gamma t}. \tag{16}$$

Then, the linearized system of Eqs. (1)–(4) in the nonrelativistic limit can be cast in a second order differential equation for the inductive electric field E_x which, e.g., in the nonrelativistic limit, reads

$$\frac{\partial}{\partial y}\left\{ [2v_0^2(y) - \gamma^2] \ \frac{\partial}{\partial y} E_x \right\} + \gamma^2(\gamma^2 + 2)E_x = 0, \tag{17}$$

where $v_0(y) = v_{0,1}(y)$. If $\gamma < \gamma_{\max}$, where $\gamma_{\max}$ is the maximum growth rate computed for a uniform plasma with the largest value of $v_0(y)$, the coefficient of the second order derivative vanishes for purely growing modes and a local Frobenius analysis [15] of Eq. (17) shows that the solution is singular at the point $\overline{y}$ where $2v_0(\overline{y})^2 = \gamma^2$. In the neighborhood of $\overline{y}$ we find

$$E_x \sim \ln|y - \overline{y}|, \tag{18}$$

which leads to

$$B_z \sim (y - \overline{y})^{-1}. \tag{19}$$

The logarithmic singularity in E_x is mathematically analogous to the one which is encountered at the Alfvén resonance in the case of shear-Alfvén waves propagating in a weakly inhomogeneous plasma (see, e.g., Refs. [16,17] and, for general oscillations in inhomogeneous flows [18]). The singularity in the spatial dependence of B_z indicates that the magnetic field generated by the Weibel instability in a nonuniform plasma is strongly inhomogeneous, and that it is localized in the neighborhood of the resonant point. Around this point the field reverses its polarity, which corresponds to the formation of a current sheet.

IV. TIME EVOLVING SIMULATIONS

We investigate the occurrence, the location, and the evolution of ''resonant'' modes by numerical integration of the normalized two-electron-fluid equations (1)–(4). We model the inhomogeneous equilibrium electron velocity as

$$\mathbf{v}_{0,1}(y) = v_\infty + \frac{\delta}{2}[1 + \tanh(y/l)]\mathbf{e}_x,$$

$$\mathbf{v}_{0,2} = -\mathbf{v}_{0,1}, \tag{20}$$

where $1/l$ is the dimensionless equilibrium gradient parameter. Then, $v_{0,1}(y \to -\infty) = v_\infty$, $v_{0,1}(y \to +\infty) = v_\infty + \delta$, and we integrate Eqs. (1)–(4) in the interval $y = [-L_y, L_y]$, $L_y/l = 70$, with the following boundary conditions for all the variables:

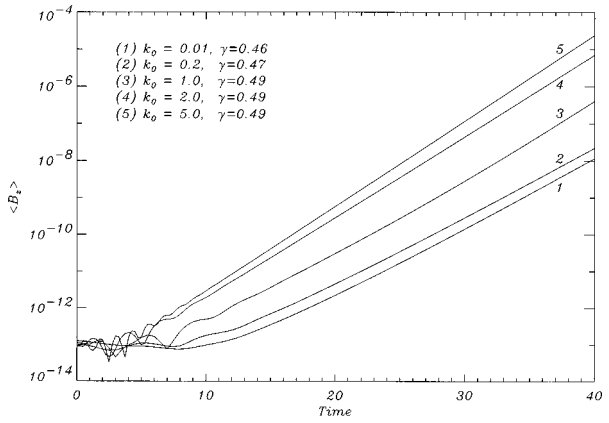

FIG. 3. Mean amplitude of the magnetic field $\langle B_z \rangle$ versus time with $v_\infty = 0.25$ and $\delta = 0.25$ for five different values of the initial wave number, $k_0 = 0.01, 0.2, 1, 2, 5$. All these curves refer to 1D nonrelativistic inhomogeneous simulations.

$$\frac{\partial}{\partial y} = 0 \quad \text{at } y = \pm L_y. \tag{21}$$

The numerical initial value code is described in the Appendix; it has been optimized for massively parallel computers and runs presently on the Connection Machine 200 of the Scuola Normale of Pisa and on the Connection Machine 5 of the Institut de Physique du Globe of Paris.

At the time $t = 0$ with $v_\infty = 0.25$ and $\delta = 0.25$ [see Eq. (20)], we perturb the equilibrium fields with a very small disturbance on each of the physical quantities. The initial perturbations are of the form $f_j(y, t=0) = 10^{-6}\exp[-y^2/\sigma]\sin(k_0 y + \phi_j)$, where ϕ_j is a random phase and $\sigma = 80/l$. These perturbations decay rapidly for $|y| > 9/l^{1/2}$ well outside the inhomogeneous region. We define the mean amplitude of the perturbation as

$$\langle f \rangle(t) = \left[\frac{1}{2L_y} \int_{-L_y}^{L_y} f(y,t)^2 \ dy \right]^{1/2}. \tag{22}$$

We have performed a number of simulations for different values of the wave vector of the initial perturbation $0.01 \leqslant k_0 \leqslant 5$ and of the inhomogeneity scale length $0.1 < l < 10$.

It is worth stressing that $k_0 \simeq 1$ corresponds approximately to the typical spatial scale for which the growth rate of the corresponding homogeneous mode with $v_{0,1} = \max(v_{0,1}(y))$ saturates at its maximum value (see Fig. 1). We define this scale as $k_{\text{sat}}^{\text{hom}}$.

In Fig. 3 we plot the mean amplitude of the magnetic field for different values of k_0 ($\delta = 0.25$, $l = 1$, and $v_\infty = 0.25$) and in Fig. 4 we show the spatial behavior of the magnetic field for $k_0 = 0.2$ at different times. Nonlinear effects start coming into play at $t \simeq 50$. In Fig. 5 we plot the magnetic field versus y for the same run of Fig. 4 at time $t = 0$ (dashed line) and overplot the magnetic field at later times every $\Delta t = 0.5$ (continuous lines). Each curve is normalized to its maximum absolute value.

For ''small'' initial wave numbers, $k_0 < 1$, the most interesting result is the dynamical formation of a strong peak of the magnetic field B_z in the central inhomogeneous region

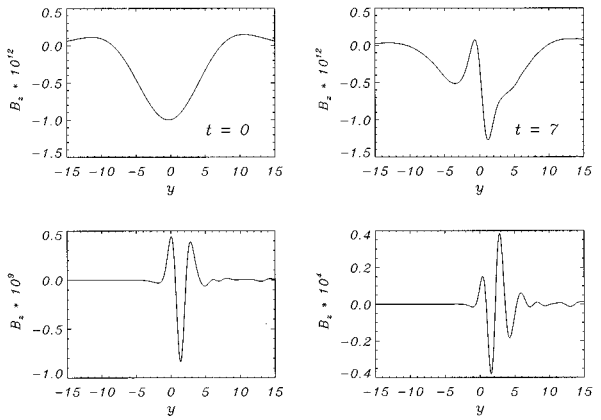

FIG. 4. Dependence of the magnetic field B_z on y in a nonrelativistic case (corresponding to curve 2 of Fig. 3) at different times, $t=0,7,25,40$. The values of the parameters are: $k_0=0.2$, $v_\infty=0.25$, $\delta=0.25$.

near $y=0$ where the equilibrium gradients are maximum (see Fig. 4). This process develops on a characteristic (dimensionless) time $t_{pk}\sim 5$ which depends on the value of the inhomogeneity scale length l, while it is independent of the particular choice of k_0. This characteristic time is much shorter than the inverse of the growth rate corresponding to the initial wave number of the perturbation.

Eventually the typical scale length of the perturbation becomes of $O(1)$ (i.e., $k\sim k_{\rm sat}^{\rm hom}$) and the small scale formation process rapidly slows down. Then the mean amplitude $\langle B_z\rangle(t)$ grows according to a time dependence that is very close to an exponential one (see Fig. 3). The estimated growth rate γ [obtained by an exponential best fit of $\langle B_z(t)\rangle, t>t_{pk}$] is independent of k_0, as shown in Fig. 1 (stars). The resulting ''resonant'' mode does not propagate significantly, as shown in Fig. 5, so that we can assume that the frequency of the mode is small or zero. The peak of $B_z(y,t)$ is located near the point where $2v_0^2-\gamma^2=0$, as expected from the local analysis of Eq. (17).

After the initial rapid generation of the peak ($t_{pk}\sim 5$), the small scale formation process slows down, but continues at a

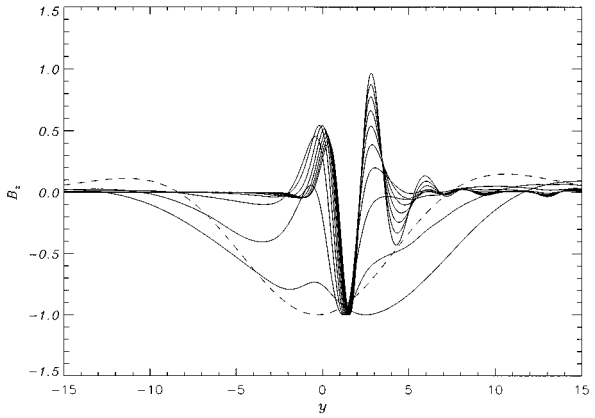

FIG. 5. Evolution of the dependence of the magnetic field B_z on y in the same case as in Fig. 4 from $t=0$ to $t=50$ showing the absence of propagation. The dashed line corresponds to the initial condition $B_z(t=0)$. Each curve is normalized to its maximum absolute value.

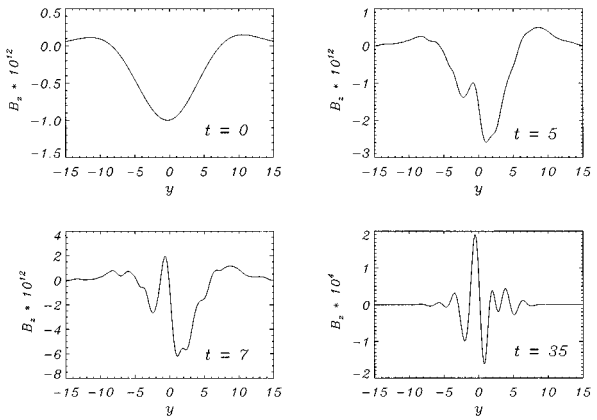

FIG. 6. Dependence of the magnetic field B_z on y in a relativistic 1D case at different times, $t=0,5,7,35$. The values of the parameters are $k_0=0.2$, $\delta=0.25$, $v_\infty=0.749$.

finite rate. This result is not surprising because of the lack of a physical dissipation mechanism in the adopted equations; moreover, the numerical dissipation of our numerical scheme is negligible until the typical spatial scale of the perturbation becomes comparable with the grid spacing. This is far from being the case in our simulations.

For larger values of the wave number ($k_0\geqslant 1$) our numerical results show that the small scale formation process is less evident since the spatial scale of the initial perturbation is of the same order or even smaller than the scale which is reached by the resonance during the initial ''fast'' process ($t<t_{pk}$) observed when $k_0<1$. Thus, when $k\geqslant k_{\rm sat}^{\rm hom}$, the singularity does not play a significant role in this linear phase and the mode evolves more or less as in the homogeneous case.

The scale l of mean gradient of the electron streams, see Eq. (20), controls the characteristic time of the fast initial small scale formation. For $0.01\leqslant k_0\leqslant 0.2$, $v_\infty=0.25$, and $\delta=0.25$ we made a number of runs with $l=0.1,\ 1,\ 10$. The results of these simulations can be summarized as follows. The characteristic time of small scale formation (pinching process) depends on the initial inhomogeneity of the electron streams as $t_{\rm pinch}=t_0 l^{1/2}$; on the other hand, the characteristic spatial scale reached by the system, $k\sim k_{\rm sat}^{\rm hom}$, is independent of l and, as observed for a fixed value of the inhomogeneity scale ($l=1$), independent of k_0. Similar results on the formation and structure of the resonant modes have been obtained for nonsymmetric electron streams.

In order to study the resonant Weibel instability in the relativistic regime, we have performed a number of runs which show the same qualitative behavior observed in the nonrelativistic regime. In Fig. 6, as an example, we show the formation of the resonance by plotting the magnetic field versus y at different times. The parameters used in this run are $k_0=0.2$, $v_\infty=0.749$, $\delta=0.25$, and the growth rate is $\gamma=0.65$.

The formation of a Weibel resonance is also evident for 2D modes which lead to the formation of a chain of oppositely polarized magnetic domains and to current density vortices. This is shown in Figs. 7–9. In Fig. 7 we show the shaded contours of the magnetic field at four times, $t=0,7,25,40$. Whiter and darker regions correspond to larger values of the magnetic field with opposite polarity; in the

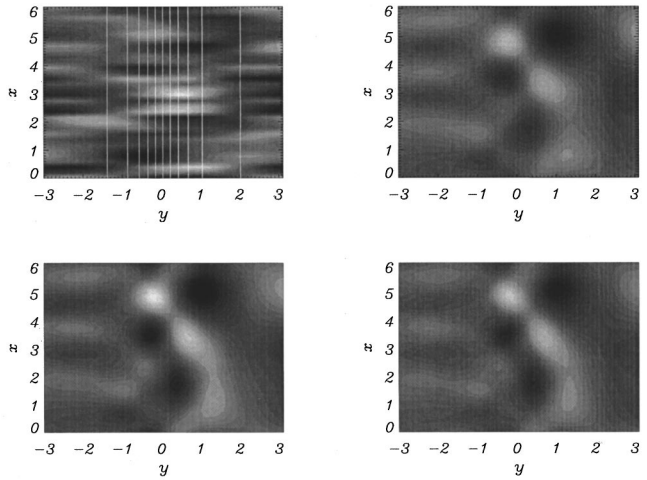

FIG. 7. Shaded contours of the magnetic field B_z for the 2D instability in a plasma with inhomogeneous nonrelativistic symmetric electron streams at four times, $t=0,15,25,27$. The values of the parameters are $k_x=k_y=1$, $k_0=0.2$, $\delta=0.25$, $v_\infty=0.25$. Darker regions correspond to increasingly positive values and whiter regions to increasingly negative values of the magnetic field. In the first frame white lines are the contour lines of the initial inhomogeneous velocity stream.

first frame, white lines are the contour lines of the initial inhomogeneous velocity [see Eq. (20)]. Notice that the y interval in this figure (and in Figs. 8 and 9) is much narrower than in the 1D simulations, Figs. 4–6. In Fig. 7 we note that the characteristic y length of the magnetic field generated by the pinching process in the inhomogeneous region is of the same order of that observed in 1D simulations. In Fig. 8 we show the shaded contours of (A) E_x and (B) E_y and of the densities of the two electron populations, frames (C) and (D), at $t=27$. It is worth noticing that in Fig. 8 the densities of the two electron streams form narrow spatial structures (filamentation) but, at this stage, their velocities do not develop vortices that are only seen in their weighted sum (i.e., in the

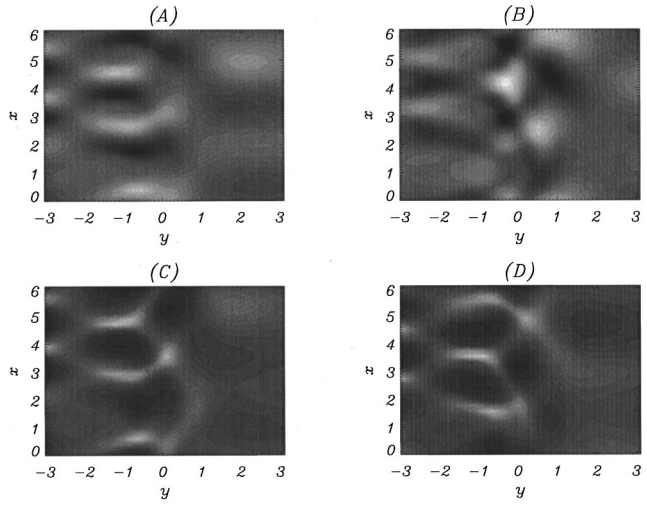

FIG. 8. Shaded contours at $t=27$ of the electric field components E_x and E_y [frames (A) and (B)] and of the two electron densities n_1 and n_2 [frames (C) and (D)]. Parameters are the same as in Fig. 7.

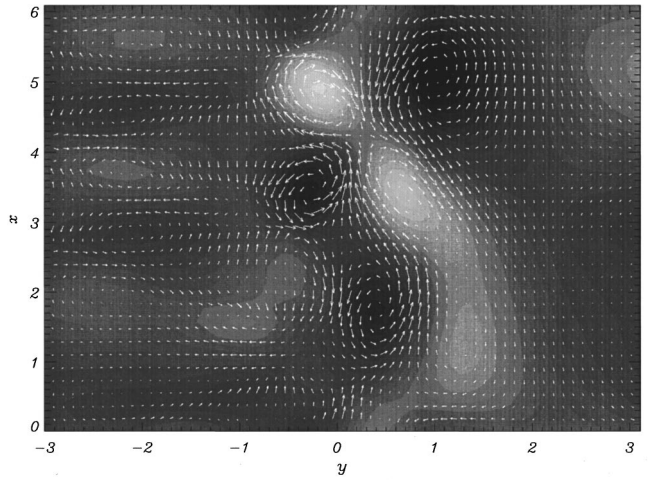

FIG. 9. Enlarged representation of the contours of the magnetic field B_z at $t=25$ with the same colors as in Fig. 7. The arrows represent the direction of the electron current density.

current density). The current vortices at $t=25$ are shown in Fig. 9 (white arrows) together with the shaded contour magnetic field (same colors of Fig. 7).

V. CONCLUSIONS

We have performed a linear analysis of the 1D and 2D spatial structure and time evolution of the Weibel instability in a plasma with nonuniform counterstreaming electron streams. We have found, both analytically and numerically, that this instability develops a resonance-type spatial structure and that the generated magnetic field is highly localized and reverses its polarity at the resonant position. We have shown that the resonance occurs roughly around the point where the gradient of the stream velocity is largest. In the case of 1D perturbations, a current layer is formed very rapidly at the resonance position, almost independently of the characteristic scale of the initial perturbation. In 2D a chain of current vortices is formed. The spatial scale of the magnetic field continues to decrease until nonlinear effects and/or three-dimensional effects leading to magnetic line reconnection induced by electron inertia [19], both not included in the present analysis, become dominant. Magnetic reconnection can be expected to play an important role in the evolution of the X points that are produced by the 2D instability. A vivid example of a magnetic X point is indeed shown in Fig. 9.

ACKNOWLEDGMENTS

We thank G. Bertin, A. Mangeney, F. Pantellini, G. Einaudi, and M. Velli for many fruitful discussions. We are pleased to acknowledge the Scuola Normale Superiore of Pisa for the use of their CM200 and Institut de Physique du Globe of Paris for the use of their CM5.

APPENDIX

The numerical code directly integrates Eqs. (1)–(4). It advances in time with the explicit algorithm ADAMS BASHFORD III with fixed time step δt and an accuracy $\sim O(\delta t^3)$.

Defining $\mathbf{R}_l^n$, $l=1,\ldots,4$ the right hand side of each of the equations (1)–(4) at the time n and assuming that $\mathbf{R}_l^n$, $\mathbf{R}_l^{n-1}$, $\mathbf{R}_l^{n-2}$ are known, the algorithm calculates the fields at the new time as follows:

$$\mathbf{H}_l^{n+1}=\mathbf{H}_l^n+\delta t\left[\frac{23}{12}\mathbf{R}_l^n-\frac{4}{3}\mathbf{R}_l^{n-1}+\frac{5}{12}\mathbf{R}_l^{n-2}\right], \quad \text{(A1)}$$

$$\mathbf{H}_1=\mathbf{p}_a, \quad H_2=n_a, \quad \mathbf{H}_3=\mathbf{E}, \quad H_4=B_z. \quad \text{(A2)}$$

To calculate the spatial derivatives, in the x direction we use fast Fourier transforms with periodic boundary conditions. In the inhomogeneous y direction we use a rather different technique described as follows. First of all, it is of particular importance that during the simulation the boundary conditions do not influence significantly the evolution of the instability, and that the inhomogeneous region ($|y|\leqslant 5$) where strong gradients are generated must be ''well resolved.'' Therefore we make use of a nonregular (physical) grid on an interval much larger than all the characteristic lengths of the system with an increasing density of grid points in the central region. The physical nonuniform y mesh is transformed into an equispaced numerical s mesh according to

$$y(s)=\frac{s}{\gamma}-\alpha\cdot\tanh\left(\frac{s}{\beta}\right). \quad \text{(A3)}$$

On the numerical equispaced mesh s the derivatives are calculated using compact finite differences (see [20], and references therein) the computational cost of which is larger than that of classical finite differences; but these differences allow one to obtain an accurate resolution of a wide range of spatial scales (not far from spectral methods) while keeping the flexibility of all finite difference methods for nonperiodic situations. In our code, we use the eighth order pentadiagonal scheme with an accuracy

$$\epsilon=\frac{16}{9!}ds^8\frac{d^9f}{ds^9}. \quad \text{(A4)}$$

Near the boundaries, at the points $i=2$ and $i=N-1$, the scheme is reduced to a tridiagonal one, always on an equispaced centered mesh, with an accuracy $\epsilon\sim ds^4$. At the boundaries in the points $i=1,N$ we directly introduce the boundary conditions, Eq. (21).

[1] E. W. Weibel, Phys. Rev. Lett. **2**, 83 (1959).
[2] R. L. Morse and W. Nielson, Phys. Fluids **14**, 830 (1971).
[3] R. C. Davidson, D. A. Hammer, I. Haber, and C. E. Wagner, Phys. Fluids **15**, 317 (1972).
[4] M. Ogasawara and A. Hirao, J. Phys. Soc. Jpn. **50**, 990 (1981).
[5] P. Yoon, Phys. Fluids B **1**, 1336 (1989).
[6] T. Yang, Y. Gallant, J. Arons, and A. Langdon, Phys. Fluids B **5**, 3369 (1993).
[7] A. S. Kingsep, K. V. Chubar, and V. V. Yan'kov, in *Reviews of Plasma Physics*, edited by B. Kadomtsev (Consultants Bureau, New York, 1990), Vol. 16, p. 243.
[8] V. Yu. Bychenkov *et al.*, Zh. Éksp. Teor. Fiz. **98**, 1269 (1990) [Sov. Phys. JETP **71**, 709 (1990)].
[9] G. A. Askar'yan, S. V. Bulanov, F. Pegoraro, and A. M. Pukhov, Pis'ma Zh. Éksp. Teor. Fiz. **60**, 240 (1994) [JETP Lett. **60**, 251 (1994)].
[10] G. A. Askar'yan, S. V. Bulanov, F. Pegoraro, and A. M. Pukhov, Comments Plasma Phys. Control. Fusion **10**, 173 (1995).
[11] C. S. Wu, P. Yoon, L. F. Ziebell, C. Chang, and H. K. Wong, J. Geophys. Res. **97**, 141 (1992).
[12] A. Lui, P. Yoon, and C. Chang, J. Geophys. Res. **98**, 153 (1993).
[13] P. Yoon and A. Lui, J. Geophys. Res. **101**, 4899 (1996).
[14] F. Pegoraro, S. V. Bulanov, F. Califano, and M. Lontano, Phys. Scr. **T63**, 262 (1996).
[15] C. M. Bender and S. A. Orszag, *Advanced Mathematical Methods for Scientists and Engineers* (McGraw-Hill, New York, 1978), p. 70.
[16] A. Hasegawa and C. Uberoi, *The Alfvén Wave*, DOE Critical Review Series (U.S. Dept. of Energy, Washington, DC, 1982).
[17] G. Bertin, G. Einaudi, and F. Pegoraro, Comments Plasma Phys. Control. Fusion **17**, 35 (1986).
[18] A. V. Timofeev, Usp. Fiz. Nauk **102**, 185 (1970) [Sov. Phys. Usp. **13**, 632 (1971)].
[19] S. V. Bulanov, A. S. Sakharov, and F. Pegoraro, Phys. Fluids B **4**, 1 (1992).
[20] F. Califano, Comput. Phys. Commun. **99**, 29 (1996).